





**Pressure-induced multicriticality and electronic instability in the quasi-kagome ferromagnet URhSn**Arvind Maurya <sup>1,\*</sup>, Dilip Bhoi,<sup>2</sup> Fuminori Honda,<sup>1,3</sup> Yusei Shimizu <sup>1</sup>, Ai Nakamura,<sup>1</sup> Yoshiki J. Sato <sup>1</sup>, Dexin Li,<sup>1</sup> Yoshiya Homma,<sup>1</sup> M. Sathiskumar <sup>2</sup>, Jun Gouchi,<sup>2</sup> Yoshiya Uwatoko,<sup>2</sup> and Dai Aoki<sup>1</sup><sup>1</sup>*Institute for Materials Research, Tohoku University, Oarai, Ibaraki 311-1313, Japan*<sup>2</sup>*Institute for Solid State Physics, The University of Tokyo, Kashiwa, Chiba, 277-8581, Japan*<sup>3</sup>*Central Institute of Radioisotope Science and Safety, Kyushu University, Motoooka 744, Fukuoka 819-0395, Japan*

(Received 7 February 2021; revised 24 September 2021; accepted 21 October 2021; published 10 November 2021)

We report an unconventional class of pressure-induced quantum phase transitions, possessing two bicritical points at 6.25 GPa in URhSn. This unique transformation accompanies a Fermi surface reconstruction, demarcating competing ordered phases suitably described with a localized and itinerant description of the magnetic  $5f$  electrons. Ferromagnetic fluctuations over a wide range of temperatures and pressures in the pressure-induced low temperature phase are evidenced by a robust  $T^{5/3}$  temperature dependence of resistivity up to 11 GPa, which is a characteristic of an elusive marginal Fermi-liquid state.

DOI: [10.1103/PhysRevB.104.195119](https://doi.org/10.1103/PhysRevB.104.195119)

Pressure is proven to be an effective knob for tuning lattice-coupled competing interactions and hence revealing exotic phases and associated interesting phenomena which otherwise would have been inaccessible. Suppression of an antiferromagnetic order by pressure often leads to emergent unconventional superconductivity or non-Fermi liquid behavior in the vicinity of a putative quantum critical point (QCP), maneuvered by quantum fluctuations [1–3]. However, in the case of a ferromagnetic ground state, a generic second-order QCP is usually avoided by coupling the order parameter to fermionic soft modes [4]. This results in either the appearance of a modulated magnetic structure or switching to a first-order transition above a pressure specified by a tricritical point [4–6].

So far, only CeRh<sub>6</sub>Ge<sub>4</sub> [7,8] manifests a clean ferromagnetic (FM) QCP. There are other materials, e.g., YbNi<sub>4</sub>(P<sub>1-x</sub>As<sub>x</sub>)<sub>2</sub> [9] and CeTi<sub>1-x</sub>V<sub>x</sub>Ge<sub>3</sub> [10] reportedly showing ferromagnetic quantum criticality, but a smearing by disorder in such a substituted system cannot be denied.

A FM QCP is believed to be stabilized by reduced dimensionality, noncentrosymmetric crystal structure and large spin orbit coupling [11]. Here, we demonstrate that  $5f$ -electron system URhSn provides a novel scheme in a pressure-temperature ( $P$ - $T$ ) phase diagram of correlated electron materials.

URhSn crystallizes in ZrNiAl-type noncentrosymmetric hexagonal structure in which U atoms lie on a frustrated quasi-kagome lattice in the  $c$  plane [Fig. 1(a)] [12]. Two phase transitions occur in URhSn at temperatures  $T_O = 52$ – $58$  K and  $T_C = 16$ – $17$  K, where  $T_O$  is well characterized by a large jump in specific heat (10 J/K-mol), a sharp drop in electrical resistivity, and a feeble kink in magnetization [13–18]. Although the ground state of URhSn is ferromagnetic, the nature of the

order parameter for the phase transition at  $T_O$  remains hidden in neutron scattering [15] and <sup>119</sup>Sn Mössbauer spectroscopy [19]. A quadrupolar order or a noncollinear magnetic phase below  $T_O$  is inferred by a reinforcement of  $T_O(H)$  in magnetic fields parallel to the  $c$  axis [13]. A small Sommerfeld coefficient ( $\gamma = 12$  mJ/mol K<sup>2</sup>) in specific-heat capacity and a relatively large ordered moment of  $2.1 \mu_B/U$  observed in neutron scattering are consistent with a weak  $c$ - $f$  hybridization and nearly localized  $5f$  electrons in URhSn at ambient pressure [13,15].

The Czochralski method equipped in a tetra-arc furnace was utilized to grow the URhSn single crystal. Single crystals were annealed at 800 °C under a vacuum better than  $10^{-6}$  torr for 30 days. Although, annealing does not affect the magnetic properties of URhSn, the annealed samples showed sharper transitions at  $T_O$  and  $T_C$ , as seen by specific heat [13]. The high quality of the single crystal used for resistivity under pressure experiments was confirmed by sharp Laue spots, high residual resistivity ratio (41), and low residual resistivity ( $6.5 \mu\Omega$  cm) as well as quantum oscillations of frequencies up to 1.55 kT (see Figs. S1 and S2 of the Supplemental Material [20]). The effective mass for the largest detected Fermi surface in de Haas–van Alphen (dHvA) effect is found to be  $1.5 m_0$ , where  $m_0$  is the rest mass of an electron. We determine the Dingle temperature to be 2.0 K, which furnishes a mean free path of 1020 Å in the URhSn single crystal, assuming a spherical shape of the Fermi surface. A large mean free path further attests high quality of the single crystal. A bar-shaped sample of dimension 0.8 mm  $\times$  0.3 mm  $\times$  0.2 mm with long direction parallel to  $[11\bar{2}0]$  was obtained by means of the Laue method and a spark erosion cutting machine. For estimation of phonon contribution to resistivity, a polycrystalline sample of ThRhSn was prepared by an arc-melting process. At ambient pressure, the resistivities of URhSn and ThRhSn were measured using a commercial Quantum Design physical property measurement system. Electrical resistivity under pressure measurements in temperature range 2.5–300 K were performed in a cubic anvil pressure cell [21]. A symmetrical

\*Present address: Max Planck Institute for Solid State Research, Heisenbergstrasse 1, 70569 Stuttgart, Germany; a.maurya@fkf.mpg.de

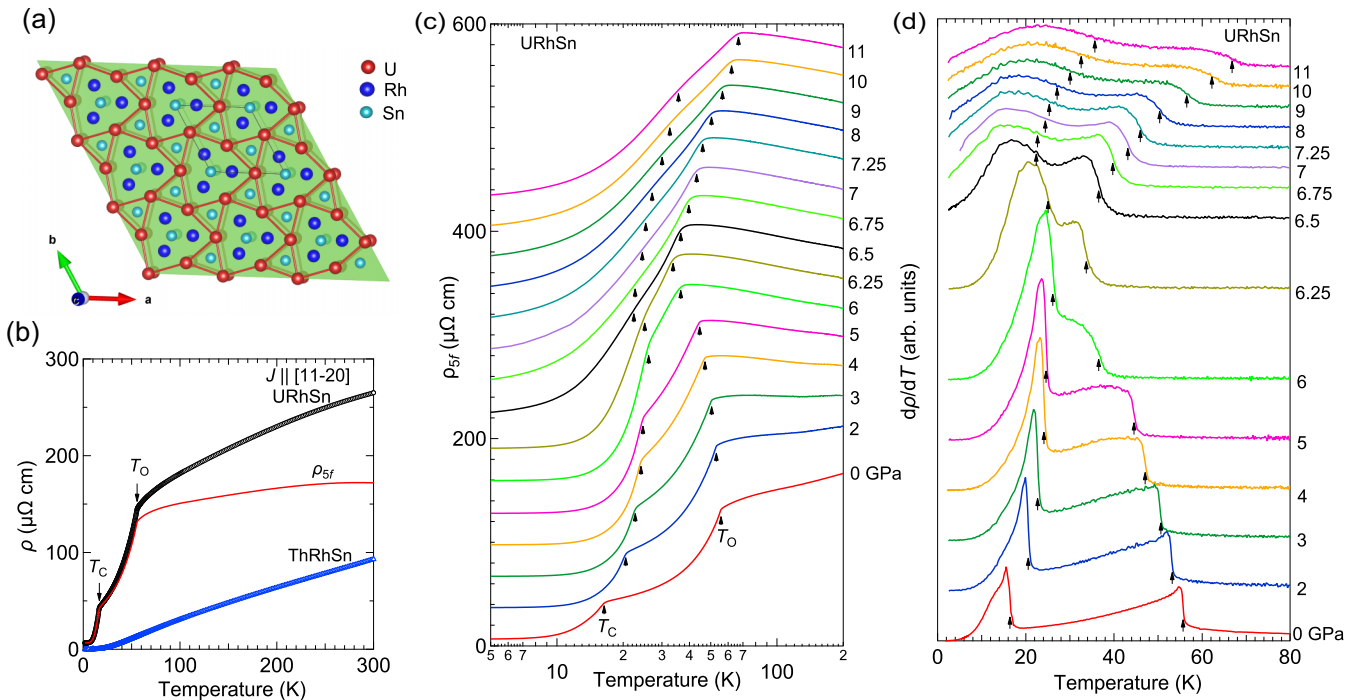


FIG. 1. (a) Crystal structure of URhSn. The triangular units of U atoms constitute a quasi-kagome lattice in the *c* plane. A sandwiching mirror plane containing Rh and Sn atoms parallel to this quasi-kagome layer is shown with translucent green color. (b) Electrical resistivity of URhSn for the current along  $[11\bar{2}0]$  direction along with of nonmagnetic analog ThRhSn. In ThRhSn case, the residual resistivity has been subtracted. The red curve is the difference of the two resistivities giving contribution from the 5*f* electrons, i.e.,  $\rho_{5f}$ . (c) Pressure dependence of  $\rho_{5f}(T)$  curves in URhSn on logarithmic temperature scale. The  $\rho_{5f}(T)$  traces measured under pressure have been shifted vertically by 30  $\mu\Omega$  cm with respect to the adjacent ones for clarity. (d) Temperature derivative of resistivity with pressure in URhSn. Vertical arrows in (c) and (d) point to the transition temperatures. See Fig. S3 of Supplemental Material [20] for the criteria used in determining  $T_O$  and  $T_C$ .

compression through six faces of the MgO gasket and *in situ* load maintenance mechanism in the cubic anvil setup ensures a nearly homogeneous transmission of pressure across the sample throughout the measurement. Pressure increments were done monotonically from 2 GPa to 11 GPa at 300 K, at which the pressure-transmitting medium Flourinert remains in a liquid state. Electrical resistance was measured by a standard four probe technique with a small current excitation of 3 mA passing along the hexagonal  $[11\bar{2}0]$  crystallographic direction. Electrical contacts on the sample with 20- $\mu$ m-thin gold wires were made with silver paste.

The double phase transitions in URhSn manifest themselves by kink anomalies followed by rapid drops in resistivity, similar to the onset of a magnetic order as shown in Fig. 1(b). The contribution of 5*f* electrons in electrical resistivity,  $\rho_{5f}$ , is obtained by subtracting other contributions mainly composed of scattering off phonons as estimated by the nonmagnetic analog ThRhSn. Below 20 K, the change in resistivity of ThRhSn remains smaller than 1  $\mu\Omega$  cm and the subtraction process does not alter the resistivity of URhSn,  $\rho$ , by more than 2%.

Figure 1(c) shows  $\rho_{5f}$  of URhSn measured at various pressures represented on a logarithmic temperature scale, assuming that the phonon contribution is unchanged under pressure. The kinks in  $\rho_{5f}(T)$  corresponding to the successive phase transitions in URhSn show their presence as steps in temperature derivative ( $d\rho/dT$ ), which can be traced up to

11 GPa, albeit above 6 GPa the anomalies at the transition temperatures broaden [Figs. 1(c) and 1(d)]. On increasing pressure,  $T_O$  decreases while  $T_C$  increases, approaching toward each other until a critical pressure,  $P_C \approx 6.25$  GPa. The minimum value of  $T_O(P)$  is 33.7 K at 6.25 GPa, while the maximum value of  $T_C(P)$  is 26.1 K in the closest vicinity; hence the two transitions remain well separated in the *P-T* plane. A hysteresis or step-like feature in  $\rho(T)$  showing a first-order behavior is absent up to 11 GPa.

$\rho_{5f}(T^2)$  below 10 K of URhSn shown in Fig. 2(a) for selected pressures reveals a remarkable evolution above 6.25 GPa, indicating a drastic change in the electronic structure. The *A* coefficient derived by fitting equation  $\rho_{5f}(T) = \rho_0 + AT^2$  between 2.5–5 K shows an abrupt increase from 0.007(5)  $\mu\Omega$  cm  $K^{-2}$  at 6 GPa to 0.249(6)  $\mu\Omega$  cm  $K^{-2}$  at 6.75 GPa [Fig. 2(b)]. Concomitantly, the residual resistivity  $\rho_0$  shows a sharp increase and plateau above 6.75 GPa. This behavior indicates a stabilization of a pressure-induced phase in which the 5*f* electrons are strongly hybridized with conduction bands.

A subquadratic behavior in  $\rho_{5f}(T)$  is a hallmark of non-Fermi liquid behavior and is ubiquitous in metallic magnets near quantum criticalities [1–3].  $\rho_{5f}$  curves in the pressure-induced phase acquire an upward curvature with  $T^2$ , indicating an emergent non-Fermi liquid phenomenon (see Figs. 2(a) and Figs. S4 and S5 of the Supplemental Material [20]). At and above 8 GPa, a linear variation with

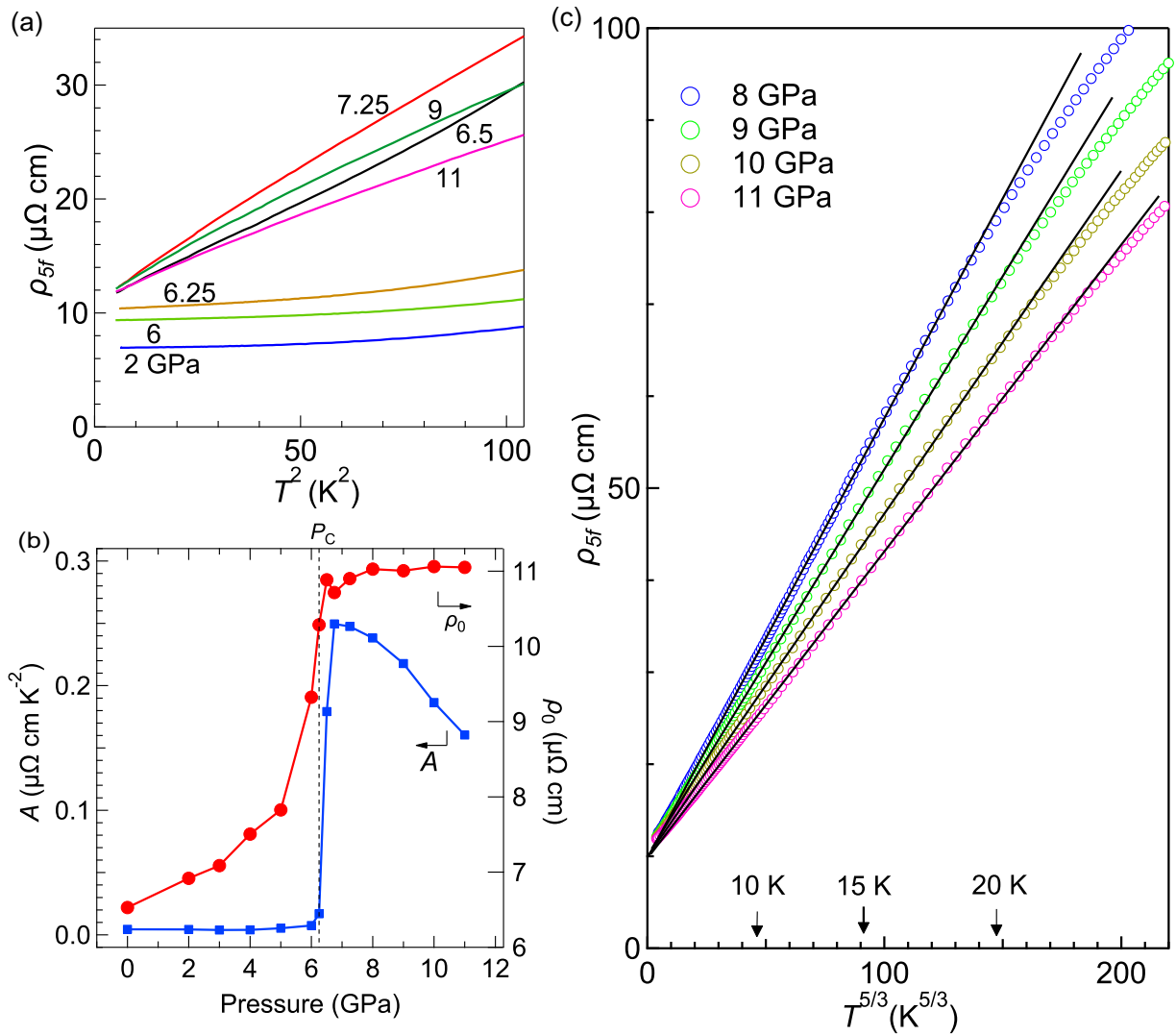


FIG. 2. (a) 5f-electron-derived resistivity of URhSn on quadratic temperature scale at selected pressures. (b) Variation of the A coefficient (left axis) and  $\rho_0$  derived from the least-squares linear fit to  $\rho_{5f}(T^2)$  curves below 5 K. The error bars in fit results are smaller than size of the symbols. (c)  $T^{5/3}$  dependence of  $\rho_{5f}$  from 8 GPa to 11 GPa demonstrating a non-Fermi liquid behavior in URhSn over a large range of temperatures and pressures. Black lines are guides to the eyes to show the agreement.

$T^{5/3}$  can be readily seen over a substantial temperature range, though a Fermi liquid behavior is restored at low temperatures (Fig. 2(c) and Fig. S5 of the Supplemental Material [20]). A similar exponent has been observed in resistivity of several itinerant electron systems, namely, URhAl [22],  $\text{U}_3\text{P}_4$  [23],  $\text{Ni}_3\text{Al}$  [24], and  $\text{Ni}_x\text{Pd}_{1-x}$  [25] close to the ferromagnetic instability as expected from the self-consistent renormalization (SCR) theory for itinerant electrons in 3D [1,26]. The low-temperature pressure-induced phase above the  $P_C$  in URhSn is identical to the ferromagnetic state in  $\text{ZrZn}_2$ , in which a  $T^{5/3}$  behavior over an extended region in the  $-T$  plane well below the Curie temperature is attributed to a non-local marginal Fermi liquid state [27–30]. Note that the electronic contribution to the resistivity in both  $\text{ZrZn}_2$  (Ref. [27]) as well as the pressure-induced phase of URhSn is dominant and non-Fermi liquid behavior with exponent 5/3 is observed irrespective of subtraction of phonon contribution from total resistivity in the low temperature region below 20 K.

The magnetic and electronic phases are represented in the  $P$ - $T$  phase diagram of URhSn in Fig. 3(a). The bicritical points associated with  $T_0$  and  $T_C$  are represented by points A (6.25 GPa, 33.7 K) and B (6.25 GPa, 25.1 K), respectively. The line joining A and B extrapolates to a quantum phase transition (QPT) point C at absolute zero temperature. Figure 3(b) shows resistivity as a function of pressure,  $\rho(P)$ , at various temperatures derived from isobaric thermal scans. The onset of step in  $\rho(P)$  at  $P_C$  at low temperatures, which transforms into a sharp peak above B, is indicative of a first-order nature of the phase boundary ABC. This pressure-induced first-order phase transformation becomes a crossover above A, which is noticed up to room temperature. Hence,  $\rho(P, T)$  of URhSn consistently suggests a QPT at 6.25 GPa between competing magnetic and electronic structures.

Another interesting aspect in the phase diagram of URhSn is a coupled response of  $T_0$  and  $T_C$  with pressure, despite being well separated in temperature and apparently possessing distinctive order parameters. It is noteworthy that

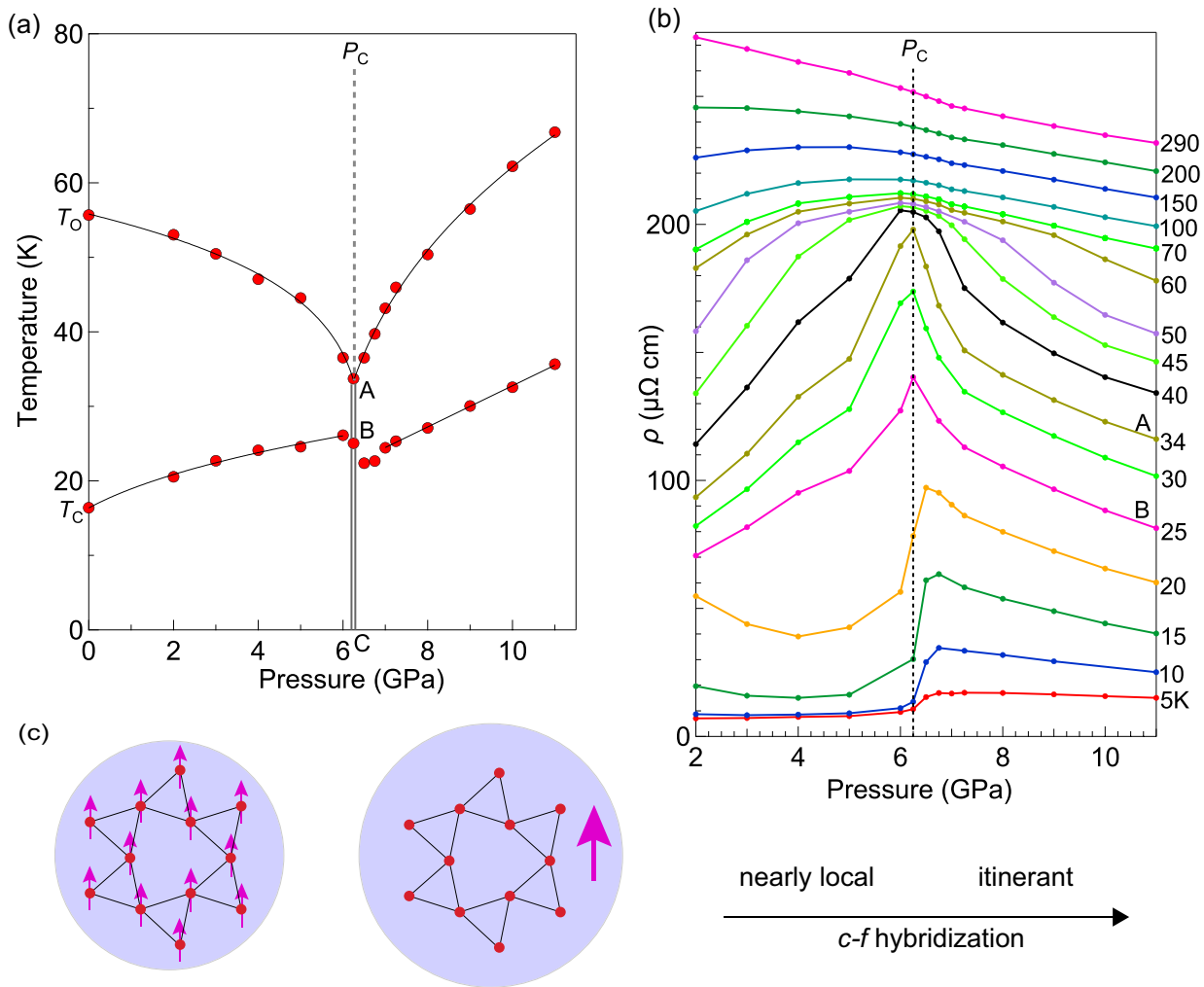


FIG. 3. (a)  $P$ - $T$  phase diagram of URhSn showing variation of  $T_C$  and  $T_0$  with pressure up to 11 GPa. The vertical grey double-line ABC represents a plausible first-order phase boundary, which is revealed by sharp anomalies in pressure dependence of resistivity in (b). This first-order phase boundary changes into a crossover above A, shown by a dashed line. Putatively, A and B are bicritical points, while C is a quantum phase transition point. (b) Traces showing isothermal variation of resistivity with pressure in URhSn derived from  $\rho(T)$  scans. (c) An illustration showing plausible electronic and magnetic ground states in the two pressure regimes across the  $P_C$ . The magnetic electrons attached nearly locally to the quasi-kagome uranium lattice become fully itinerant by pressure-induced  $c$ - $f$  hybridization above the  $P_C$ . The blue enclosures represent size of the Fermi surfaces in the two regimes.

a quadratic drop in resistivity between  $T_0$  and  $T_C$  gradually linearizes with pressure, with a slope that maximizes at  $P_C$  (see Fig. S6 of the Supplemental Material [20]). The role of the undetermined order parameter at  $T_0$  remains an open question in the unusual  $P$ - $T$  phase diagram of URhSn.

A QPT, by definition, is a phase transformation happening at absolute zero temperature and is mediated by quantum fluctuations, which is supported by the experimental data in Figs. 2(b), 2(c) and 3(b). Of course, we do not have resistivity measurements at very close to absolute zero temperature but down to fairly enough low temperatures on a reduced temperature scale ( $t = (T_C - T)/T_C$ ). More concrete information about the phases between which the transition takes place requires further exploration, e.g., by neutron scattering, and is left for future work. The multicritical behavior in URhSn is peculiar because the tuning parameter here is pressure,

which (unlike magnetic field for the case of bicriticality in YbAgGe [31]) is a non-symmetry-breaking thermodynamic quantity.

Now we discuss perhaps the most astounding novelty in a  $P$ - $T$  phase diagram illustrated by URhSn. The nature of  $f$ -electronic states as well as the associated QPTs have been a matter of long debate. Initial theories of QPTs were stemmed from itinerant electron spin fluctuation models which propose the so-called spin-density wave (SDW) scenario [32,33]. It deals with a continuous tuning of long-range SDW order set in itinerant electrons to absolute zero temperature. This scheme works under the framework of SCR theory, which predicts a  $T^{5/3}$  behavior in resistivity by itinerant ferromagnetic fluctuations close to a FM QPT for 3D case. Under another universality class, a Kondo breakdown scenario was proposed for QPTs accompanying a Fermi surface reconstruction in some  $f$ -electron materials [34–39]. Note that, in both

cases, a pressure-induced QPT demarcates a magnetically ordered state from a phase with no magnetic order, in sharp contrast to the case in URhSn. At ambient pressure, URhSn exhibits nearly local moment magnetism. Under the influence of  $c$ - $f$  hybridization introduced by pressure, it transforms into a phase that can be suitably described as an itinerant ferromagnet after a jump in the Fermi-surface volume at  $P_C$  [Fig. 3(c)]. A QPT in an  $f$ -electron system with two bicritical points separating magnetic phases across it and involving a Fermi surface reconstruction provides a channel to explore the ferromagnetic QPT both experimentally and theoretically. An interplay of competing orders with geometric or magnetic frustration inherent in the quasi-kagome lattice is a potential

cause for the unique magnetic and electronic instability. Our results show that a QPT in an  $f$ -electron system is a more general phenomena than previously thought and may involve multicritical points.

We thank V. Taufour, M. Yokoyama, Y. Tokunaga, H. Harima and Y. Ōnuki for fruitful discussions. We thank S. Nagasaki for her technical support during high-pressure experiments. We acknowledge financial support from JSPS KAKENHI Grants No. JP18F18017, No. JP19H00648, No. JP15H05882, No. JP15H05886, No. JP15K21732, JP15H05884, JP19H00646, No. JP19J20539, No. JP17K14328, and No. JP20K03851.

- [1] H. Löhneysen, A. Rosch, M. Vojta, and P. Wölfle, *Rev. Mod. Phys.* **79**, 1015 (2007).
- [2] C. Pfleiderer, *Rev. Mod. Phys.* **81**, 1551 (2009).
- [3] G. R. Stewart, *Rev. Mod. Phys.* **73**, 797 (2001).
- [4] D. Belitz, T. R. Kirkpatrick, and T. Vojta, *Phys. Rev. Lett.* **82**, 4707 (1999).
- [5] M. Brando, D. Belitz, F. M. Grosche, and T. R. Kirkpatrick, *Rev. Mod. Phys.* **88**, 025006 (2016).
- [6] U. S. Kaluarachchi, S. L. Bud'ko, P. C. Canfield, and V. Taufour, *Nat. Commun.* **8**, 546 (2017).
- [7] B. Shen, Y. Zhang, Y. Komijani, M. Nicklas, R. Borth, A. Wang, Y. Chen, Z. Nie, R. Li, X. Liu, H. Lee, M. Smidman, F. Steglich, P. Coleman, and H. Yuan, *Nature (London)* **579**, 51 (2020).
- [8] H. Kotegawa, E. Matsuoka, T. Uga, M. Takemura, M. Manago, N. Chikuchi, H. Sugawara, H. Tou, and H. Harima, *J. Phys. Soc. Jpn.* **88**, 093702 (2019).
- [9] A. Steppke, R. Küchler, S. Lausberg, E. Lengyel, L. Steinke, R. Borth, T. Lühmann, C. Krellner, M. Nicklas, C. Geibel, F. Steglich, and M. Brando, *Science* **339**, 933 (2013).
- [10] W. Kittler, V. Fritsch, F. Weber, G. Fischer, D. Lamago, G. Andr, and H. v. Löhneysen, *Phys. Rev. B* **88**, 165123 (2013).
- [11] T. R. Kirkpatrick and D. Belitz, *Phys. Rev. Lett.* **124**, 147201 (2020).
- [12] A. Dwight, *J. Less-Common Met.* **34**, 279 (1974).
- [13] Y. Shimizu, A. Miyake, A. Maurya, F. Honda, A. Nakamura, Y. J. Sato, D. X. Li, Y. Homma, M. Yokoyama, Y. Tokunaga, M. Tokunaga, and D. Aoki, *Phys. Rev. B* **102**, 134411 (2020).
- [14] V. Tran, R. Troć, and D. Badurski, *J. Alloy. Compd.* **219**, 285 (1995).
- [15] F. Mirambet, B. Chevalier, L. Fournes, J. F. da Silva, M. F. Ramos, and T. Roisnel, *J. Magn. Magn. Mater.* **140**, 1387 (1995).
- [16] T. Palstra, G. Nieuwenhuys, R. M. Vlastuin, J. Van den Berg, J. Mydosh, and K. Buschow, *J. Magn. Magn. Mater.* **67**, 331 (1987).
- [17] V. Tran and R. Troć, *J. Magn. Magn. Mater.* **102**, 74 (1991).
- [18] S. F. Matar, F. Mirambet, B. Chevalier, and J. Etourneau, *J. Magn. Magn. Mater.* **140**, 1389 (1995).
- [19] R. Kruk, R. Kmieć, K. Łatka, K. Tomala, R. Troć, and V. H. Tran, *Phys. Rev. B* **55**, 5851 (1997).
- [20] See Supplemental Material at <http://link.aps.org/supplemental/10.1103/PhysRevB.104.195119> for Laue pattern (Fig. S1), dHvA oscillations (Fig. S2), criteria used for determining  $T_O$  and  $T_C$  (Fig. S3), NFL behavior (Figs. S4 and S5), and pressure-induced linearization of the  $\rho_{sf}(T)$  in URhSn between  $T_O$  and  $T_C$  (Fig. S6).
- [21] N. Mori, H. Takahashi, and N. Takeeshita, *High Pressure Res.* **24**, 225 (2004).
- [22] Y. Shimizu, D. Braithwaite, B. Salce, T. Combier, D. Aoki, E. N. Hering, S. M. Ramos, and J. Flouquet, *Phys. Rev. B* **91**, 125115 (2015).
- [23] S. Araki, M. Hayashida, N. Nishiumi, H. Manabe, Y. Ikeda, T. C. Kobayashi, K. Murata, Y. Inada, P. Wiśniewski, D. Aoki, Y. Ōnuki, E. Yamamoto, and Y. Haga, *J. Phys. Soc. Jpn.* **84**, 024705 (2015).
- [24] P. G. Niklowitz, F. Beckers, G. G. Lonzarich, G. Knebel, B. Salce, J. Thomasson, N. Bernhoeft, D. Braithwaite, and J. Flouquet, *Phys. Rev. B* **72**, 024424 (2005).
- [25] M. Nicklas, M. Brando, G. Knebel, F. Mayr, W. Trinkl, and A. Loidl, *Phys. Rev. Lett.* **82**, 4268 (1999).
- [26] J. Mathon, *Proc. R. Soc. London, Ser. A* **306**, 355 (1968).
- [27] R. P. Smith, M. Sutherland, G. G. Lonzarich, S. S. Saxena, N. Kimura, T. Takashima, M. Nohara, and H. Takagi, *Nature (London)* **455**, 1220 (2008).
- [28] M. Sutherland, R. P. Smith, N. Marcano, Y. Zou, S. E. Rowley, F. M. Grosche, N. Kimura, S. M. Hayden, S. Takashima, M. Nohara, and H. Takagi, *Phys. Rev. B* **85**, 035118 (2012).
- [29] S. Takashima, M. Nohara, H. Ueda, N. Takeshita, C. Terakura, F. Sakai, and H. Takagi, *J. Phys. Soc. Jpn.* **76**, 043704 (2007).
- [30] F. M. Gosche, C. Pfleiderer, G. J. McMullan, G. G. Lonzarich, and N. R. Bernhoeft, *Phys. B: Condens. Matter B* **206–207**, 20 (1995).
- [31] Y. Tokiwa, M. Garst, P. Gegenwart, S. L. Bud'ko, and P. C. Canfield, *Phys. Rev. Lett.* **111**, 116401 (2013).
- [32] K. Ueda and T. Moriya, *J. Phys. Soc. Jpn.* **39**, 605 (1975).
- [33] J. A. Hertz, *Phys. Rev. B* **14**, 1165 (1976).
- [34] Q. Si and F. Steglich, *Science* **329**, 1161 (2010).
- [35] P. Coleman, C. Pépin, Q. Si, and R. Ramazashvili, *J. Phys.: Condens. Matter* **13**, R723 (2001).
- [36] Q. Si, S. Rabello, K. Ingersent, and J. L. Smith, *Nature (London)* **413**, 804 (2001).
- [37] P. Coleman and A. J. Schofield, *Nature (London)* **433**, 226 (2005).
- [38] P. Gegenwart, Q. Si, and F. Steglich, *Nat. Phys.* **4**, 186 (2008).
- [39] K. Miyake and H. Ikeda, *J. Phys. Soc. Jpn.* **75**, 033704 (2007).